NUCL SCI TECH (2019) 30:2
https://doi.org/10.1007/s41365-018-0529-3

Study of neutron production and moderation for sulfur neutron capture therapy

Meng Peng[1,2] · Guo-Zhu He[1] · Qi-Wei Zhang[1] · Bin Shi[1] · Hong-Qing Tang[1] · Zu-Ying Zhou[1]

Received: 26 March 2018 / Revised: 3 September 2018 / Accepted: 5 September 2018 / Published online: 2 January 2019

Abstract Neutron capture therapy with Sulfur-33, similar to boron neutron capture therapy with Boron-10, is effective in treating some types of tumors including ocular melanoma. The key point in sulfur neutron capture therapy is whether the neutron beam flux and the resonance capture cross section of $^{33}S(n,\alpha)^{30}Si$ reaction at 13.5 keV can achieve the requirements of radiotherapy. In this research, the authors investigated the production of 13.5 keV neutron production and moderation based on an accelerator neutron source. A lithium glass detector was used to measure the neutron flux produced via near threshold $^{7}Li(p,n)^{7}Be$ reaction using the time-of-flight method. Furthermore, the moderation effects of different kinds of materials were investigated using Monte Carlo simulation.

Keywords Sulfur Neutron capture therapy · Boron neutron capture therapy · $^{33}S(n,\alpha)^{30}Si$ resonance reaction · $^{7}Li(p, n)^{7}Be$ neutron source

✉ Meng Peng
pengmeng0417@sina.com

Guo-Zhu He
heguozhu818@126.com

[1] Key Laboratory of Nuclear Data, China Institute of Atomic Energy, Beijing 102413, China

[2] College of Liberal Arts and Sciences, National University of Defense Technology, Changsha 410073, China

1 Introduction

Shortly after the discovery of neutrons by Chadwick in 1932 [1], the principles of neutron capture therapy (NCT) were proposed by Locher [2]. A patient suffering from malignant glioma was treated using the Brookhaven Graphite Research Reactor in 1954, as the first case of boron neutron capture therapy (BNCT) [3]. BNCT may initially appear to be a complex therapy; however, the approach is in fact relatively simple. Tumor cells with a high concentration of ^{10}B can capture thermal neutrons, which results in $^{10}B(n,\alpha)^{7}Li$ reaction. The products of this capture reaction have such a high linear energy transfer (LET) in a short range (4–10 μm) that their energy deposition is limited to a single cell. Therefore, these products can selectively irradiate and kill tumor cells that absorb a sufficient amount of ^{10}B, while avoiding damage to normal, healthy cells from damage [4].

In addition to ^{10}B, an interesting isotope for NCT of cancer is ^{33}S [5], which has a large (n,α) cross section in the keV range, which is much greater than that of (n,γ) [6]. The LET for 3.1 MeV α-particles emitted by $^{33}S(n,\alpha)^{30}Si$ reaction is sufficiently large to effectively destroy cancer cells, so ^{33}S can be utilized for NCT, which is called sulfur neutron capture therapy (SNCT). C. Wagemans *et al.* (1986) [7] measured the resonance cross section of $^{33}S(n,\alpha)^{30}Si$ reaction, and the experimental result exhibited some resonances in the keV range. These resonances are illustrated in Fig. 1, where the most important resonance peak (with a cross section above 20 barns) occurs at a neutron energy close to 13.5 keV. Sulfur is an essential component of all living cells, and its concentration in cells is three orders of magnitude larger than boron. Therefore,

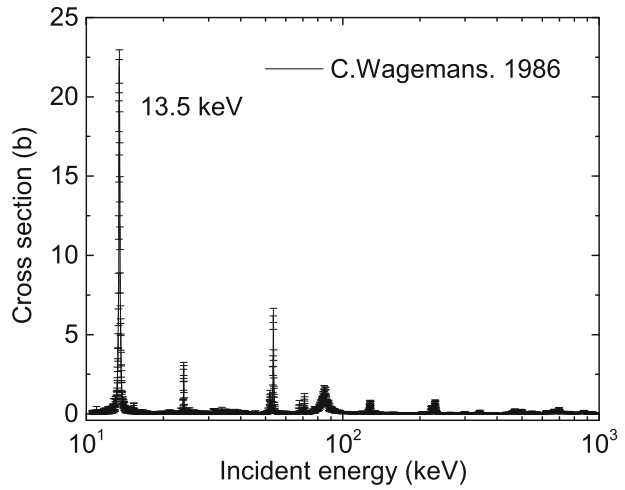

Fig. 1 Resonance structure of $^{33}S(n,\alpha)^{30}Si$

^{33}S-carriers [5] are a promising option because it results in a high local concentration in tumors. Some studies [5, 8–15] have shown an enhancement in the neutron-absorbed dose for a combination of ^{33}S and ^{10}B.

The therapeutic effect of SNCT is evaluated by estimating the biological dose, which is a common dosimetric reference for a given treatment scheme. The biological dose partly depends on the resonance cross section of $^{33}S(n,\alpha)^{30}Si$ reaction and the neutron flux and energy within the area of a lesion. Our work is devoted to designing a neutron generator for SNCT.

2 Neutron source selection

A neutron source based on a low-energy, high-current, and light ion accelerator is being developed as a potential replacement of reactors to meet the requirements of a clinical NCT facility [16]. Accelerators have several potential advantages related to safety, cost, and high neutron flux in the keV range, compared to reactor-based neutron sources for clinical radiotherapy. In this regard, they are optimal neutron sources for SNCT.

Table 1 lists the properties of several neutron-producing charged-particle reactions proposed for use in an accelerator-based neutron source [16–18]. The neutron energies via $^{9}Be(p,n)^{9}B$, $^{9}Be(d,n)^{10}B$ and $^{13}C(d,n)^{14}N$ reactions are too high to increase the resonance neutron intensity after moderation. Although $^{45}Sc(p,n)^{45}Ti$ reaction can generate quasi-monoenergetic 13.5 keV neutrons, its cross section is too small, and a small change of the proton energy leads to a great influence on the emitted neutrons. The threshold value (Eth) of $^{7}Li(p,n)^{7}Be$ reaction is 1880.57 keV, and the emitted neutron energy (about 29.68 keV) is close to the resonance energy [19]. The neutron yield of this reaction is high, and the relatively low-energy neutrons require less moderation than those generated via other reactions to enhance the 13.5 keV neutron intensity.

3 Neutron source simulation and experimental measurement

3.1 Neutron source simulation and moderation

There are many factors that affect the neutron flux via $^{7}Li(p,n)^{7}Be$ reaction such as target thickness, outgoing angle, and proton energy. In addition, with the increase in the incident proton energy, the proton has a large range, which can produce more accompanied γ-rays via $^{7}Li(p,p')^{7}Li$ and $^{7}Li(p,\gamma)^{8}Be$ reactions [20] that are the harmful biological dose. An optimal experimental scheme should be based on the balance of these three facts for neutron production and moderation.

The neutron energy and yield via near threshold $^{7}Li(p,n)^{7}Be$ reaction were investigated using TARGET [21, 22] code. In this work, two proton separation threshold energies (1.885 MeV and 1.930 MeV) and two target separation thicknesses (6.2 μm as the thin target and 152 μm as the thick target) were chosen to calculate neutron production.

In addition, different kinds of moderator materials were used to enhance the intensity of resonance neutrons. These materials should have a high scattering cross section and a low capture cross section in the keV range. They also do not exhibit decomposition in the radiation field, high long-term radioactivity or moisture during long-time operation [23]. The following materials as water (H_2O), graphite, heavy water (D_2O), and polythene (CH_2) have been suggested. The moderation effects of the aforementioned materials were calculated using the Geant4 (Version: 10.2) Monte Carlo code [24]. In this study, the geometric model was built according to the actual experimental conditions presented in Sect. 3.2, and the cylindrical moderator close to the neutron source was placed in the collimator aperture. The GGST_BERT_HP [25, 26] has been used as a standard physics model to describe neutron transportation, which employs a high-precision neutron package used for neutrons with energies below 20 MeV, down to thermal energies.

3.2 Experimental neutron source

The time-of-flight (TOF) method was used to measure the neutron beam via near threshold $^{7}Li(p,n)^{7}Be$ reactions based on the HI-13 Tandem Accelerator at the China Institute of Atomic Energy [27]. The minimum energy of

Table 1 Characteristics of charged-particle reactions considered for accelerator-based SNCT neutron source

Reaction	Bombarding energy (MeV)	Cross section (mb)	Neutron energy at 0° angle (MeV)	Target melting point (°C)	Thermal conductivity (W m^{-1} K^{-1})
$^{7}Li(p,n)^{7}B$	1.9	232	0.030	181	85
$^{9}Be(p,n)^{9}B$	4.0	120	1.060	1287	201
$^{9}Be(d,n)^{10}B$	1.5	–	2.010	1287	201
$^{13}C(d,n)^{14}N$	1.5	396	1.080	3550	230
$^{45}Sc(p,n)^{45}Ti$	2.91	3.73	0.014	1541	15.8

the proton beam generated by the accelerator was approximately 7 MeV, and the pulse length was less than 3 ns (full duration at half maximum). An aluminum slice with a thickness of 280 μm was used as the absorber to reduce the proton energy to a mean energy of 2.5 MeV.

Although $^{7}Li(p,n)^{7}Be$ reaction is favorable for enhancing neutron intensity in the keV range, some difficulties are still encountered when lithium is used as an ideal target. As shown in Table 1, the low melting point and poor thermal conductivity of pure lithium make it a poor candidate. A good water-cooling system is essential for the timely removal of heat from the target, otherwise the integrity of the lithium target will be compromised. The chemical properties of lithium cause it to rapidly react with air to form compounds, which directly affects the neutron energy and yield. During the fabrication and installation of the lithium target, it is not allowed to come into contact with air [16].

A schematic of the experimental setup is shown in Fig. 2. A lithium glass detector (ϕ 1.6 cm × 0.95 cm) used to monitor the neutron beam was positioned at 0° with respect to the proton beam axis. The detector signals were used to trigger a time-to-digital converter (TDC) to reduce dead time, while the delayed signals of proton beams were recorded for data acquisition of neutron flight time. Two parameters were registered simultaneously for each event: the pulse height (PH) and the TOF. The detection efficiency of the lithium glass detector was previously calibrated by partners [28]. The experimental parameters are summarized in Table 2.

4 Results and discussion

4.1 Simulated neutron spectra and discussion

The calculated neutron energy spectra obtained via the near threshold $^{7}Li(p,n)^{7}Be$ reaction under different conditions are shown in Fig. 3, and the neutron yields under the different energy ranges are shown in Table 3. The neutron spectra at 0° angle have an obvious peak at 30 keV, while the resonance neutron yields are very small. Compared with the target thickness, the incident proton has a greater influence on the neutron spectra and yields. According to the TARGET results, the neutron energy spectrum corresponding to the 0° output angle in Fig. 3d was selected to study neutron moderation at a high flux.

The moderation effects of different kinds of materials were calculated using the Geant4 code; the results are shown in Fig. 4. The resonance neutron yields increased gradually with the thickness of the moderators until there was a dynamic balance between the neutron absorption and moderation. Graphite could sufficiently moderate fast neutrons (> 30 keV) in order to enhance the intensity of the 13.5 keV neutrons, while the hydrogen-containing materials slowed down more neutrons to epithermal energies. The resonance neutron yields in the 12.6–15.8 keV range could reach 6.45×10^{5} sr^{-1} μA^{-1}, 6.93×10^{5} sr^{-1} μA^{-1}, 1.29×10^{6} sr^{-1} μA^{-1} and 5.97×10^{5} sr^{-1} μA^{-1}, respectively. According to the calculated results, graphite is an optimal moderator to generate more resonance neutrons.

4.2 Experimental neutron spectrum and discussion

A two-dimensional spectrum of "PH-TOF" based on the measured raw data is provided to allow for the discrimination of the n-γ signals, as shown in Fig. 5. The region labeled peak-1 corresponds to 240 keV neutrons because of the high detection efficiency of the lithium glass detector. The region labeled peak-2 corresponds to the 560 keV neutrons produced by the 2.5 MeV protons at the surface of the lithium target. The neutron flight distance was so short that these neutrons (< 20 keV) could not be discriminated using the TOF method. They were therefore treated as fast neutrons (> 700 keV) produced in the next pulse because their flight times were longer than that of the proton pulse period. According to the calculated results, the neutron peak at 30 keV should be clearly visible. In fact, the recorded neutron flux was moderated by the water used to cool the lithium target.

We can obtain the neutron energy spectrum by combining the two-dimensional spectrum (Fig. 5) and the detection efficiency of the lithium glass after ticking out

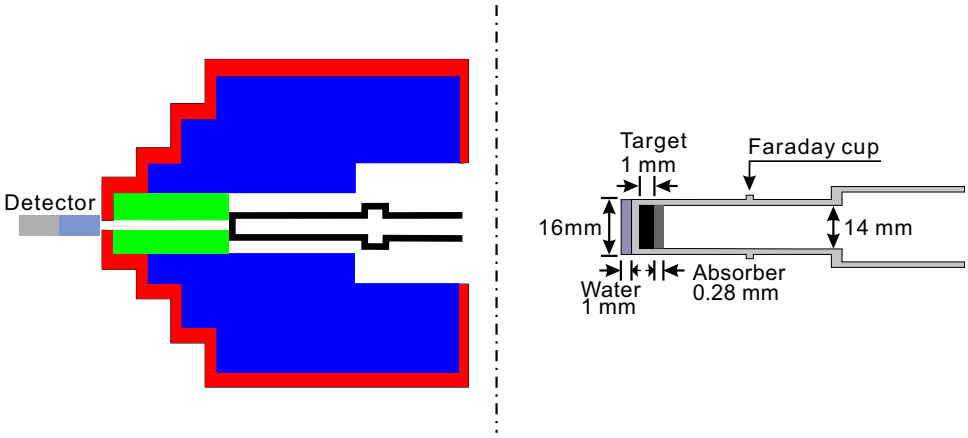

Fig. 2 (Color online) The experimental setup. Left figure shows the profile of the neutron source shield and collimator system, and right figure shows the structure of the lithium target

Table 2 Experimental parameters

Experimental condition	Value
Proton energy (MeV)	7
Averaged current (nA)	100
Repetition frequency (MHz)	3
Absorber thickness (μm)	280
Detector volt (V)	− 2020
Detector type	Lithium glass
Neutron flight distance (cm)	58.0

the γ-ray background, as shown in Fig. 6. The right peak corresponds to the region labeled peak-2 in Fig. 5, while the left peak corresponds to the approximately 180 keV neutrons produced by the 1.9–2.0 MeV proton beams. There are three issues that affect these low-energy proton beams: (1) The energy of protons after the absorber was broadened and the spectrum followed a Gaussian distribution (Full Width at Half Maximum $>$ 0.5 MeV); (2) the energy loss of protons in the Li target leads to low-energy neutrons (approximately 180 keV) production; (3) these neutrons could be produced via ^{7}Li(p, n)^{7}Be* reaction ($Eth = 2.373$ MeV).

According to the experimental results, the neutron flux reached 1.41×10^{3} sr^{-1} μA^{-1} at a distance of 58 cm from the lithium target. Moreover, the neutron source strength reached 4.74×10^{6} sr^{-1} μA^{-1}, which is lower than the calculated results by an order of magnitude. The difference is mainly attributed to the moderation and absorption of the cooling water, scattering, and absorption of the collimator.

With the experimental neutron flux, the same moderators were chosen to study the moderation effects. The Geant4 simulation results are shown in Fig. 7. The resonance neutron yield values in the 12.6–15.8 keV range could reach 4.76×10^{4} sr^{-1} μA^{-1}, 1.23×10^{5} sr^{-1} μA^{-1}, 5.23×10^{4} sr^{-1} μA^{-1} and 4.76×10^{4} sr^{-1} μA^{-1}, respectively. It is possible to obtain more 13.5 keV neutrons with deuteron-containing materials compared to those that contain carbon and hydrogen. However, none of these materials were capable of fully moderating the maximum number of fast neutrons (hundreds of keV) down to the desired resonance energy range, while increasing the resonance neutron yield. A high incident proton energy is adverse to neutron production and moderation in terms of increasing the resonance neutron yield near the threshold of ^{7}Li(p, n)^{7}Be reaction. This is an essential requirement for further SNCT neutron source studies.

5 Conclusion

^{33}S can be used for NCT because it has a large (n,α) cross section, and the emitted α-particles produce a large energy deposition near the interacting site to kill tumor cells. The key aspect of SNCT depends partially on the resonance cross section of $^{33}\mathrm{S}(\mathrm{n},\alpha)^{30}\mathrm{Si}$ reaction and the resonance neutron flux. In this study, we built a ^{7}Li(p,n)^{7}Be reaction accelerator-based neutron source for SNCT. The energy and intensity of the neutrons were measured using a lithium glass detector based on the TOF method. We also studied the optimal moderation scheme to enhance the intensity of the resonance neutrons. Using a simple moderator material can increase the 13.5 keV neutron flux, but it still has a large share of the high-energy neutrons in the neutron beam. Composite materials may be the best candidate to slow down more high-energy neutrons to enhance the resonance neutrons.

The combination of a near threshold ^{7}Li(p,n)^{7}Be reaction neutron source and the use of graphite for the production of neutron beams is potentially promising for SNCT. To achieve the best therapeutic effect, this approach needs to be studied further to obtain quasi-monoenergetic 13.5 keV neutron beams (for SNCT), or neutron beams with a maximum energy of 13.5 keV (combined SNCT

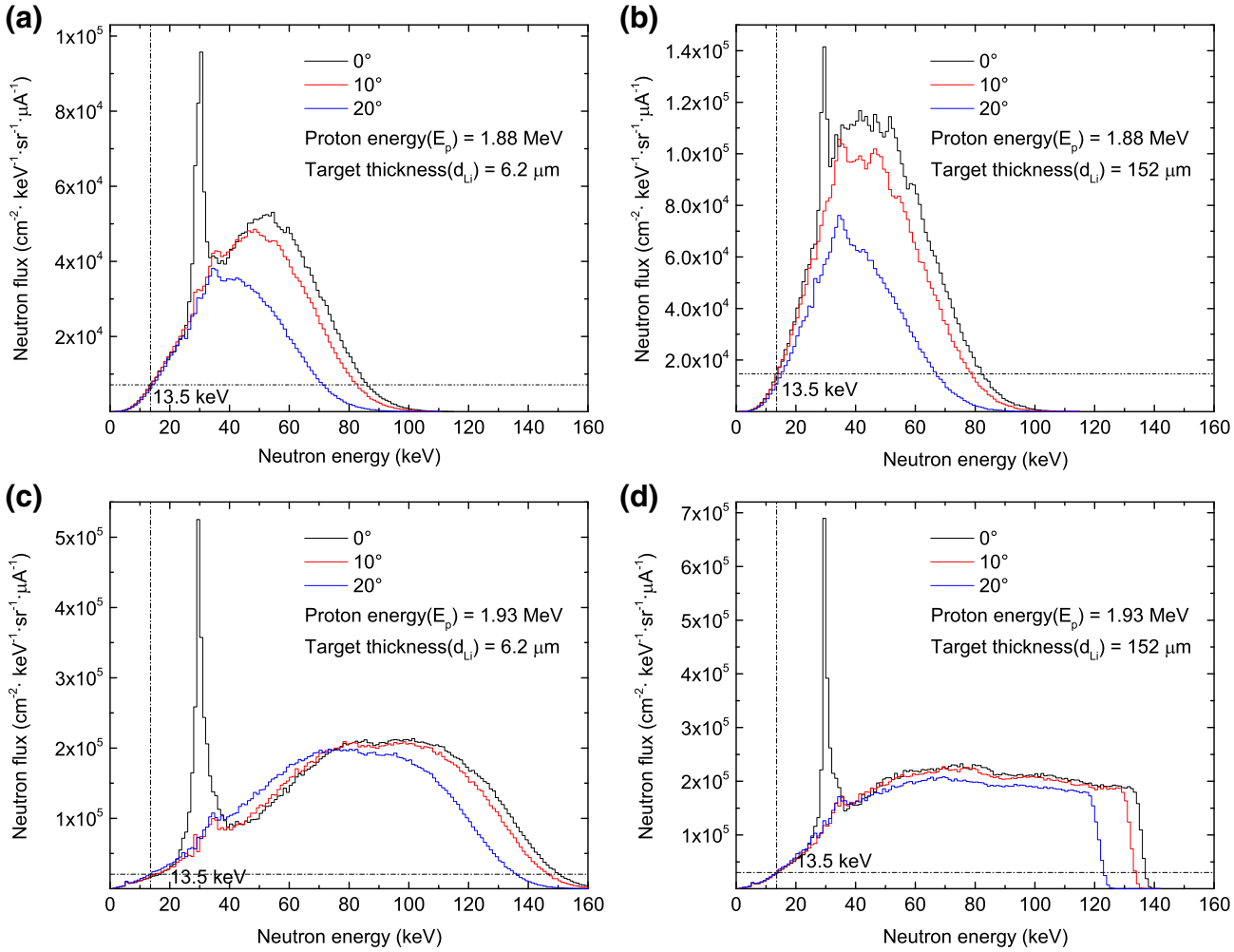

Fig. 3 (Color online) The neutron energy spectra via ^{7}Li(p,n)^{7}Be reaction under different conditions. **a** represents the conditions of 1.88 MeV proton beams and a thick target (6.2 μm), **b** represents the conditions of 1.88 MeV proton beams and a thick target (152 μm), **c** represents the conditions of 1.93 MeV proton beams and a thick target (6.2 μm), **d** represents the conditions of 1.93 MeV proton beams and a thick target (152 μm)

Table 3 Neutron flux in different energy ranges via ^{7}Li(p,n)^{7}Be reaction

Proton energy (MeV)	Target thickness (μm)	Output angle (°)	Total neutron yield (sr^{-1} μA^{-1})	Neutron yield ($\leq$ 30keV) (sr^{-1} μA^{-1})
1.885	6.2	0	2.64×10^{6}	5.22×10^{5}
		10	2.19×10^{6}	3.58×10^{5}
		20	1.44×10^{6}	3.27×10^{5}
	152	0	5.24×10^{6}	1.03×10^{6}
		10	4.29×10^{6}	8.39×10^{5}
		20	2.50×10^{6}	6.65×10^{5}
1.930	6.2	0	2.03×10^{7}	1.97×10^{6}
		10	1.79×10^{7}	7.77×10^{5}
		20	1.61×10^{7}	8.70×10^{5}
	152	0	2.39×10^{7}	2.39×10^{6}
		10	2.15×10^{7}	1.35×10^{6}
		20	1.84×10^{7}	1.45×10^{6}

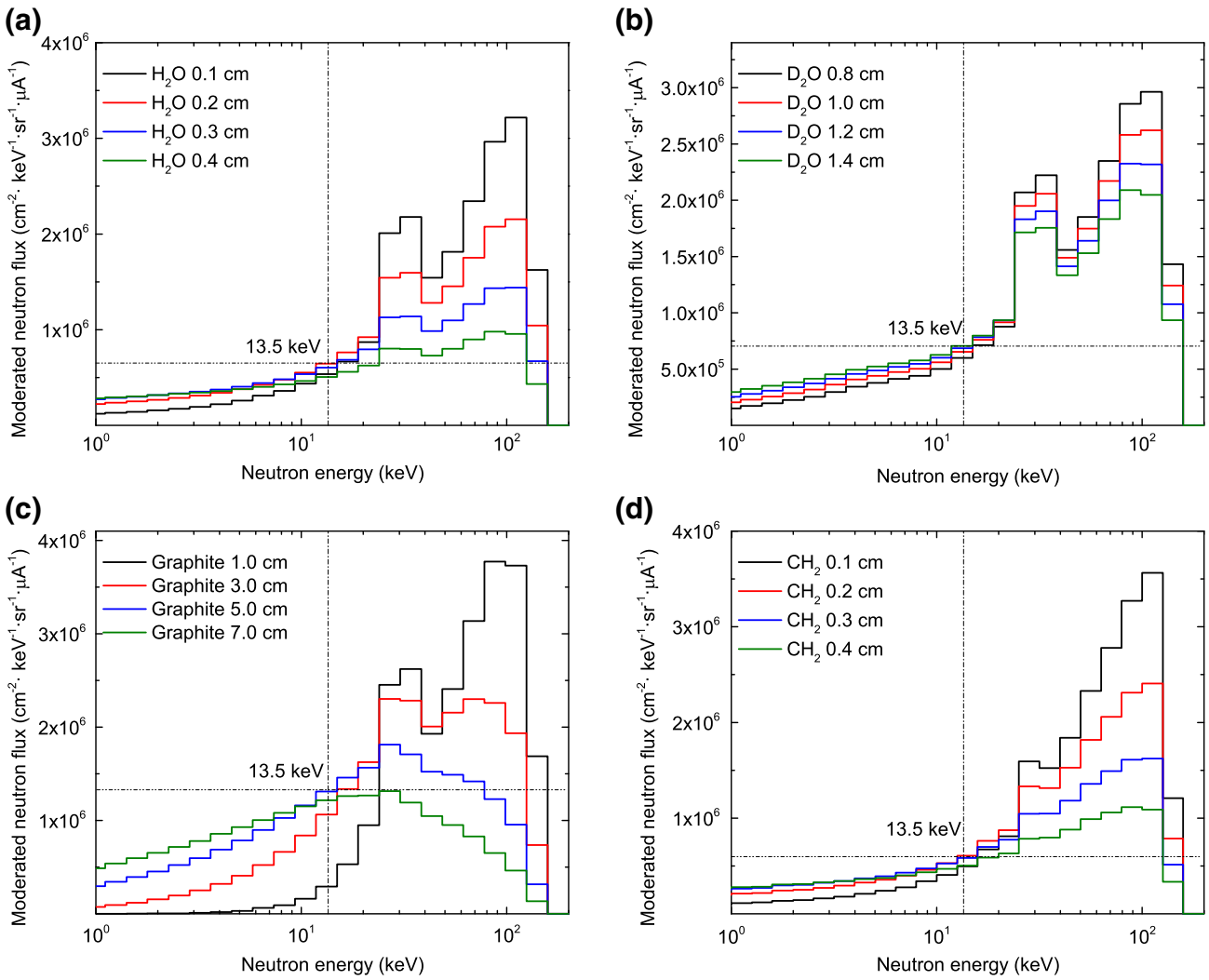

Fig. 4 (Color online) The neutron energy spectra after **a** H_2O, **b** D_2O, **c** Graphite, and **d** CH_2 moderation of different thicknesses with calculated neutron flux

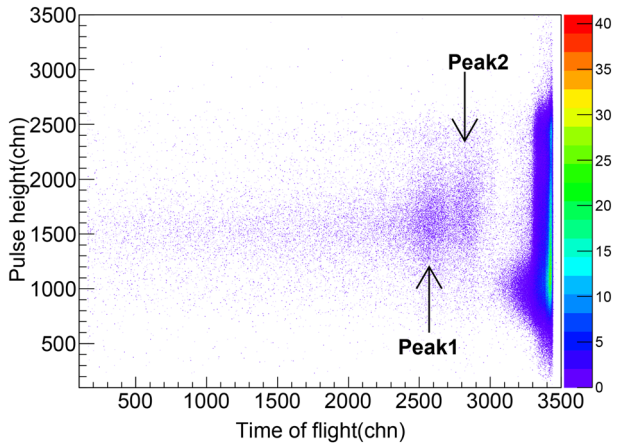

Fig. 5 (Color online) The two-dimensional spectrum of "PH-TOF" measured with lithium glass

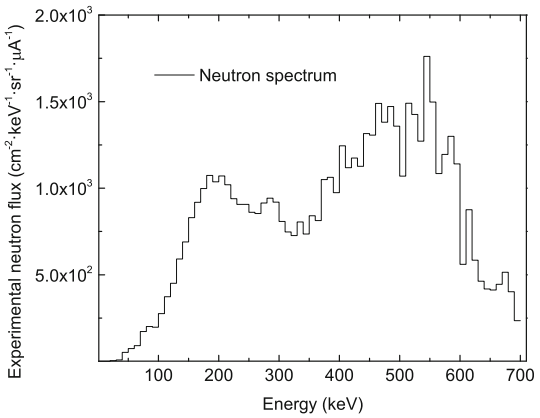

Fig. 6 Final neutron energy spectrum

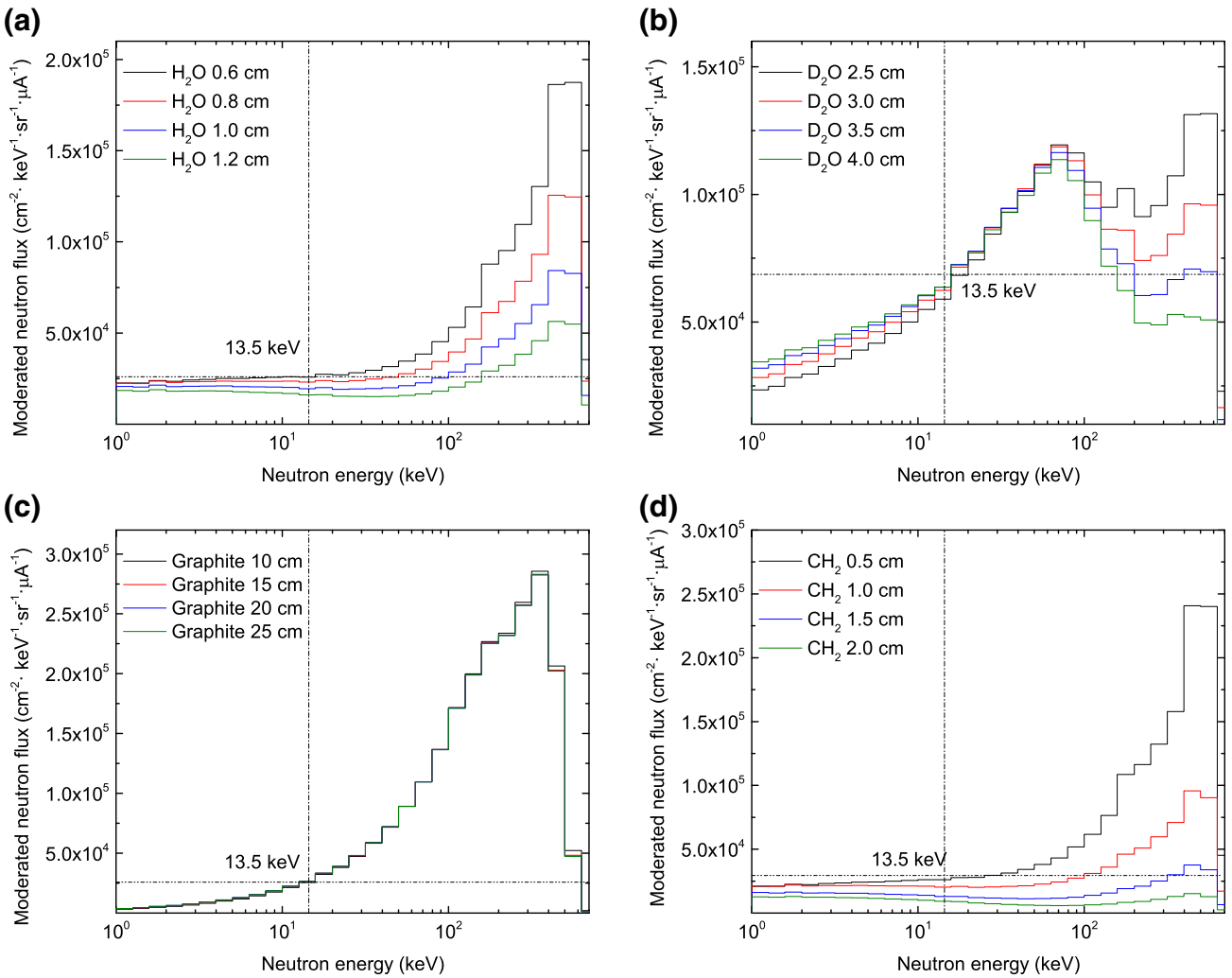

Fig. 7 (Color online) The neutron energy spectra after **a** H_2O, **b** D_2O, **c** graphite, and **d** CH_2 moderation of different thicknesses with experimental neutron flux

with BNCT). There are some discrepancies in the experimental data for $^{33}S(n,\alpha)^{30}Si$ reaction [7, 29, 30] in the keV range. This neutron source can potentially be used to clarify the existing discrepancies.

References

1. J. Chadwick, The existence of a neutron. Proc. R. Soc. **136**, 692 (1932). https://doi.org/10.1098/rspa.1932.0112
2. G.L. Locher, Biological effects and the therapeutic possibilities of neutrons. Am. J. Roentgenol. **36**, 1 (1936)
3. L.E. Farr, W.H. Sweet, H.B. Locksley et al., Neutron capture therapy of gliomas using boron. Trans. Am. Neurol. Assoc. **13**, 110 (1954)
4. R.L. Moss, Critical review, with an optimistic outlook, on boron neutron capture therapy (BNCT). Appl. Radiat. Isot. **88**, 2 (2014). https://doi.org/10.1016/j.apradiso.2013.11.109
5. I. Porras, Sulfur-33 nanoparticles: a Monte Carlo study of their potential as neutron capturers for enhancing boron neutron capture therapy of cancer. Appl. Radiat. Isot. **69**, 1838 (2011). https://doi.org/10.1016/j.apradiso.2011.04.002
6. M. Sabaté-Gilarte, J. Praena, I. Porras et al., Measurement of the $^{33}S(n,\alpha)$ cross section at n_TOF(CERN): applications to BNCT. Rep. Pract. Oncol. Radiother. **21**, 113 (2016). https://doi.org/10.1016/j.rpor.2014.08.007
7. C. Wagemans, H. Weigmann, R. Barthelemy, Measurement and resonance analysis of the $^{33}S(n,\alpha)$ cross section. Nucl. Phys. A **469**, 497 (1987). https://doi.org/10.1016/0375-9474(87)90035-2
8. I. Porras, Enhancement of neutron radiation dose by the addition of sulphur-33 atoms. Phys. Med. Biol. **53**, L1 (2008). https://doi.org/10.1088/0031-9155/53/7/L01
9. I. Porras, J. Praena, M. Sabatégilarte et al, $^{33}S(n,\alpha)$ cross section measurement at n_TOF: implications in neutron capture therapy. http://digital.csic.es/handle/10261/123302
10. J. Praena, M. Sabaté-Gilarte, I. Porras et al., ^{33}S as a cooperative capturer for BNCT. Appl. Radiat. Isot. **88**, 203 (2014). https://doi.org/10.1016/j.apradiso.2013.12.039
11. I. Porras, P.L. Esquinas, M.G. Feldmann et al., A potential selective radiotherapy for ocular melanoma by sulfur neutron capture, in *16th International Congress on Neutron Capture Therapy (ICNCT-16)* , Helsinki, Finland, June 14–19 (2014)

12. J. Praena, Experimental study of the 13.5 keV resonance of the ^{33}S(n,α)^{30}Si reaction at CERN n_TOF fa-cility for BNCT, in *16th International Congress on Neutron Capture Therapy (ICNCT-16)*, Helsinki, Finland, June 14–19 (2014)
13. I. Porras, M. Sabaté-Gilarte, J. Praena et al., ^{33}S for neutron capture therapy: nuclear data for Monte Carlo calculations. Nucl. Data Sheets **120**, 246 (2014). https://doi.org/10.1016/j.nds.2014.07.058
14. M. Sabaté-Gilarte, The ^{33}S(n,α)^{30}Si cross section measured at n_TOF Experimental Area 2(CERN): from thermal to the resolved resonance region, in *International Nuclear Data Conference for Science and Technology (ND2016)*, Bruges, Belgium , September 11–16 (2016)
15. M. Sabaté-Gilarte, J. Praena, I. Porras et al., Measurement of the ^{33}S(n,α) cross section at n_TOF(CERN): applications to BNCT. Reports Prac. Onco. Radio **21**, 113 (2016). https://doi.org/10.1016/j.rpor.2014.08.007
16. T.E. Blue, J. Yanch, Accelerator-based epithermal neutron sources for boron neutron capture therapy of brain tumors. J. Neuro-Oncol. **62**, 19 (2003)
17. D.M. Minsky, A.J. Kreiner, Near threshold ^{7}Li(p, n)^{7}Be reaction as neutron source for BNCT. Appl. Radiat. Isot. **106**, 68 (2015). https://doi.org/10.1016/j.apradiso.2015.07.038
18. K.V.K. Iyengar, S.K. Gupta, K.K. Sekharan et al., Fluctuations in the integrated cross section of the reaction ^{45}Sc(p, n)^{45}Ti. Nucl. Phys. A **96**, 521 (1967). https://doi.org/10.1016/0375-9474(67)90602-1
19. M.S. Herrera, G.A. Moreno, A.J. Kreiner et al., New method to evaluate the ^{7}Li(p, n)^{7}Be reaction near threshold. Nucl. Instrum. Meth. B **349**, 64 (2015). https://doi.org/10.1016/j.nimb.2015.01.080
20. R. Mateus, A.P. Jesus, B. Braizinha et al., Proton-induced γ-ray analysis of lithium in thick samples. Nucl. Instrum. Meth. B **190**, 117 (2002). https://doi.org/10.1016/S0168-583X(01)01222-8
21. D. Schlegel, Target User's Manual. Abteilung Ionisierende Strahlung Laborbericht (2005)
22. D. Schlegel, S. Guldbakke, *Why do We Need Target?* (Springer, Berlin, 2001), p. 881
23. IAEA-TECDOC-1223, Current Status of Neutron Capture Therapy, (International Atomic Energy Agency, Austria, 2001)
24. Geant4 Collaboration, User's Guide: For Application Developers (2015). http://geant4.web.cern.ch/geant4/UserDocumentation/UsersGuides/ForApplicationDeveloper/BackupVersions/V10.2/fo/BookForAppliDev.pdf
25. Geant4 Collaboration, Physics Reference Manual (2015). http://geant4.web.cern.ch/geant4/UserDocumentation/UsersGuides/PhysicsReferenceManual/fo/PhysicsReferenceManual.pdf
26. C.L. Lan, M. Peng, Y.Z. et al., Geant4 simulation of ^{238}U(n,f) reaction induced by D-T neutron source. Nucl. Sci. Tech. **28**, 8 (2016). https://doi.org/10.1007/s41365-016-0158-7
27. B. Yang, X. Guan, X. Cao et al., Progresses in the project of upgrading HI-13 tandem accelerator at CIAE. Nucl. Tech. **31**, 41 (2008). **(in Chinese)**
28. Q.W. Zhang, G.Z. He, X.C. Ruan et al., Calibration of neutron detection efficiency of li-glass detector. Nucl. Phys. Rev. **34**, 2460 (2013). https://doi.org/10.11804/NuclPhysRev.30.02.156. **(in Chinese)**
29. G.F. Auchampaugh, J. Halperin, R. L. Macklin et al., Kilovolt ^{33}S(n,α_0) and ^{33} S (n,γ) cross sections: Importance in the nucleosynthesis of the rare nucleus ^{36} S . Phys. Rev. C **12**, 1126 (1975). https://doi.org/10.1103/PhysRevC.12.1126
30. P.E. Koehler, J.A. Harvey, N.W. Hill, Two detectors for (n, p) and (n,α) measurements at white neutron sources. Nucl. Instrum. Meth. A **361**, 270 (1995). https://doi.org/10.1016/0168-9002(95)00123-9